SWIFTSIN: A High-Resolution Ion Isolation Waveform for the Miniaturized Linear ion Trap Mass Spectrometer by Coarse to Fine Excitation

Xinyue Ding[1], Quan Yu[1], Xinqiong Lu[2], Xiaohao Wang[1], Xinming Huo[3, *], Xiang Qian[1, *]

1. Shenzhen International Graduate School, Tsinghua University, Shenzhen, 518055, China
2. Shenzhen Chin Instrument Co. Ltd., Shenzhen, 518055, China
3. School of Biomedical Engineering, Shenzhen Campus of Sun Yat-Sen University, Shenzhen, 518107, China

[*] Corresponding Author: qian.xiang@sz.tsinghua.edu.cn, huoxm@mail.sysu.edu.cn

ABSTRACT: To figure out the reason for the drawback of the SWIFT waveform and realize the high-resolution ion isolation on the miniaturized linear ion trap mass spectrometer, we studied the efficiency that ions can be excited under different excitation durations and amplitudes at different frequencies and compared the overlap ratios of the effective excitation frequency bandwidths of the adjacent ions. According to this, we proposed a new coarse-to-fine isolation waveform named SWIFTSIN. By superposing one or more sinusoidal waveforms on the SWIFT waveform and modulating the phases of the superposed sinusoidal waveforms, the generated SWIFTSIN waveform can achieve unit mass isolation on the miniaturized linear ion trap mass spectrometer without reducing the intensity of the target ion. The isolation ability of the SWIFTSIN waveform was verified by isolating a single isotope peak in the mixed samples.

With high sensitivity and specificity, mass spectrometry has been widely used and playing an increasingly important role in biological research, food and drug analysis, explosive detection, etc.[1-4] Compared with the large-scale instruments used in the laboratory, the miniaturized ion trap mass spectrometer is more suitable for on-site analysis because of its portability and has attracted more and more researchers' attentions.[5-8] Unfortunately, the reduction of the volume has brought a series of negative effects on instrument performance. For examples, the reduction of the ion trap size limits the capacity of ion storage, intensifies the space charge effect inside; and the reduction of the radio frequency (RF) power supply volume limits the maximum RF voltage. These will ultimately bring negative impacts on the resolution, sensitivity, and ion detection range of the miniaturized ion trap mass spectrometer.[9-12]

Broadband waveform excitation is an important technology that can be applied to improve the analytical performance of the miniaturized ion trap mass spectrometer. The purpose of the technology is to activate the trapped ions selectively, which is also called ion isolation. By trapping and isolating the ion of interest and wiping out all other ions before scanning, the space charge effect can be significantly reduced, the signal-to-noise ratio, the analytical sensitivity, and the quantitative analysis ability of mass spectrometry can be improved.[13, 14] Tandem mass spectrometry is also an important way of mass spectrometry analysis.[15-17] In this mode, a specific mass-to-charge ratio ion can be isolated first, and then the target ion can be fragmented through collision-induced dissociation to obtain more abundant fragment information of the precursor ion. Accurate material identification can be obtained through such method. In the above processes, isolation can simplify the information of the tandem mass spectrum and help to further establish the relationship between the target ion and the productions.[18-20] High-resolution ion isolation tandem mass spectrometry can also be used to predict the molecular formula of the compound and obtain the breaking pathway of the compound; this is an important analysis function mainly set in large-scale mass spectrometers, [21, 22] but seldom reported in miniaturized instruments.

The commonly used broadband waveform excitation technology is the stored waveform inverse Fourier transform (SWIFT) technology,[23-27] others include filtered noise field technology [28, 29] and mixed frequency modulation technology.[30, 31] The common feature of the waveforms generated by these techniques is that they all contain specific frequency components which correspond to the secular frequencies of the ions that shouldn't be isolated, to achieve the selective excitation of the ions with different mass-to-charge ratios. The SWIFT waveform is generated by a specific amplitude spectrum through secondary phase modulation in the frequency domain and then inverse Fourier transform to the time domain.[32-34] Although the SWIFT waveform is widely used, it also has some disadvantages. When applied to the

miniaturized ion trap mass spectrometer, the isolation resolution of the SWIFT waveform is insufficient. Due to the reduction of the overall volume of the miniaturized ion trap mass spectrometer, the amplitude of the RF voltage is also limited, and as a consequence, the q value of the ion operating point is low, which will make the secular frequency interval between the adjacent ions smaller, especially for the ions with high mass-to-charge ratios.[19, 35] Therefore, when an attempt is made to isolate a target ion with a narrow isolation window, the energy of the adjacent frequency components used to excite the other ions may cause the false excitation of the target ion and greatly reduce the intensity.

Many attempts have been taken to achieve the high-resolution isolation of the target ion.[18, 35, 36] However, these methods greatly increase the complexity of the analysis sequence or increase the duration of the whole analysis sequence, which is detrimental to the on-site detection. Here, we explored the excitation of the ions under different excitation durations and amplitudes at different frequencies and obtained the absorption frequency bandwidths of the ions with different mass-to-charge ratios under these excitation conditions, and then proposed a measurement of effective excitation frequency bandwidths. We suggested that only frequency components near the isolation point will affect the isolation resolution finally and found that when the absorption frequency bandwidths of the adjacent ions overlap less, it was easier to achieve high-resolution isolation. Accordingly, a simple yet efficient isolation waveform SWIFTSIN was proposed for the high-resolution isolation of the target ion. The waveform was achieved by superposing one or more sinusoidal waveforms whose frequencies were set near the isolation point on the traditional SWIFT waveform and adjusting the phases of the superposed sinusoidal waveforms. The duration of each frequency of the sinusoidal waveform was longer than that of each frequency in the SWIFT waveform, but the amplitude was lower, thus achieving a "softer" and “coarse-to-fine” excitation effect. Our results indicated that the unit mass isolation of the target ion can be achieved with almost no loss of the target ion intensity. The MS/MS spectrum of the fragmented ions obtained after such high-resolution isolation method can also be purified. Thus, the proposed SWIFTSIN waveform is expected to improve the on-site analytical ability of the miniaturized mass spectrometer.

EXPERIMENTAL SECTION

Instrumentation. Experiments were performed on a custom-made linear ion trap mass spectrometer with a continuous atmospheric pressure interface. The distance between the field center and the surface of the two electrodes was 4 mm and 4.25 mm. The RF voltage and auxiliary AC excitation signal were applied on the two pairs of hyperbolic electrodes, respectively. Using a two-stage vacuum chamber, the first vacuum chamber had a small ion funnel for ion transmission, the RF frequency was 929 kHz. The ion trap was in the second vacuum chamber, the RF frequency was 1227 kHz. A Rotary Vacuum pump RVD-2 (pumping speed 120 L/min, KYKY Technology Co., Ltd，Beijing, China), and an Hipace 80 turbo molecular pump (pumping speed 67 L/s, Pfeiffer Vacuum, Asslar, Germany) were used to extract the vacuum. Finally, the pressure in the second vacuum chamber could be maintained at ~0.12 pa. A group of entrance lenses, serving as an einzel lens was placed between the ion trap and the skimmer located in between the two vacuum chambers. The isolation waveform could be generated by the Matlab program, downloaded to the main control board, and finally converted to the analog signal output by a 14-bit digital-analog converter. In our experiments, the normal scan rate was about 500^{Th}/s, and the duration of the isolation waveform was 21 ms. For more detail descriptions of the instrumentation, it can be referred to our previous works.[37, 38]

Chemical Samples. The chemical samples used in this study included dioxopromethazine hydrochloride, rotundine, rosiglitazone, pioglitazone, and repaglinide. All the samples were purchased from J&K Technology Co., Beijing, China, and were diluted in methanol to final concentrations of ~1mg/L.

Waveform Calculation. The SWIFT waveform and the SWIFTSIN waveform were calculated and applied in the isolation experiments. The core idea of the SWIFT waveform

design is the inverse Fourier transform. The notch frequency band of the magnitude spectrum is designed according to the secular frequency of the isolated ion, and the phase is modulated according to the quadratic phase modulation algorithm, finally, the isolation waveform is generated by inverse Fourier transform. The magnitude spectrum of the SWIFT waveform is generally conceived as a rectangular amplitude spectrum. Assuming that the amplitude of the rectangular spectrum is A_0, the corresponding SWIFT waveform is[14, 33]

$$f(t)=\frac{A_0}{2\pi}\int_{-\infty}^{+\infty}e^{jp(\omega)}e^{j\omega t}d\omega, \tag{1}$$

where $p(\omega)$ is the phase function. The quadratic phase function can be expressed as

$$p(\omega)=-\frac{1}{2}\frac{(\omega-\omega_0)^2(t_1-t_0)}{\omega_1-\omega_0}-t_0\omega, \tag{2}$$

where ω_0 to ω_1 is the frequency range of the SWIFT waveform, and t_0 to t_1 is the time duration. Figure 1a plots a SWIFT waveform with a frequency band from 0 kHz to 600 kHz and a notch from 220 kHz to 240 kHz. The duration is 21ms. Figure 1b plots the magnitude spectrum, and Figure 1c plots the time-frequency spectrum. Figure 1d is a SWIFT waveform calculated with the same frequency band, but the energy is mainly concentrated in the first 15ms. Figure 1e plots the magnitude spectrum, and Figure 1f plots the time-frequency spectrum.

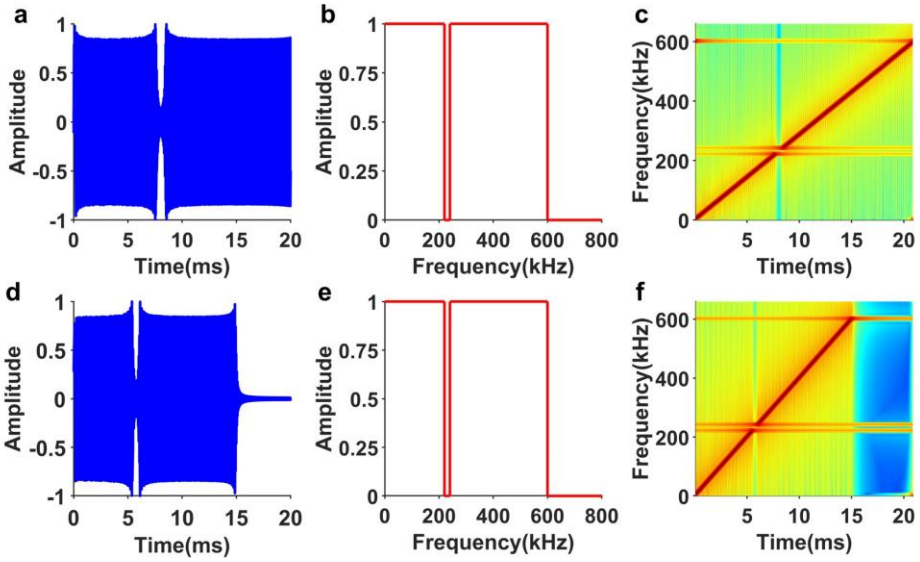

Figure 1. (a) SWIFT waveform with a notch from 220 kHz to 240 kHz. (b), (c) The magnitude spectrum and the time-frequency spectrum of the SWIFT waveform. (d) SWIFT waveform with a notch from 220 kHz to 240 kHz but the energy is mainly concentrated in the first 15ms of the duration. (e), (f) The magnitude and the time-frequency spectrum of the second SWIFT waveform.

To improve the isolation resolution of the isolation waveform, the reason why the SWIFT waveform is difficult to achieve high-resolution isolation without losing the intensity of the isolated target ion was explored and the SWIFTSIN waveform was designed. The SWIFTSIN waveform was constructed by superposing one or more sinusoidal waveforms on the SWIFT waveform. This design aimed to use a large frequency notch SWIFT waveform to achieve coarse isolation, and then use one or more sinusoidal waveforms with frequencies near the isolation point to fine excite the ions near the target ion that were not excited by the coarse isolation. The waveform contracting and superposing operations were used to avoid an increase in the detection duration. To ensure that the ions far away from the target ion were

first excited, and to reduce the influence of the space charge effect in the ion trap during the fine isolation, the SWIFT waveform was compressed to the first 15 ms in the time domain like the waveform in Figure 1d. Successively, one or more 5 ms sinusoidal waveforms were superposed between 15 ms and 20 ms of the SWIFT waveform. Thus, the total length of the designed high-resolution isolation waveform was kept same as the original SWIFT waveform. Figure 2 is a design example of a SWIFTSIN waveform. The frequency of the superposed sinusoidal waveform is 229.2 kHz. Figure 2a plots the time domain waveform of a SWIFTSIN waveform with a large notch from 220 kHz to 240 kHz. Figure 2b plots the magnitude spectrum, and Figure 2c plots the time-frequency spectrum.

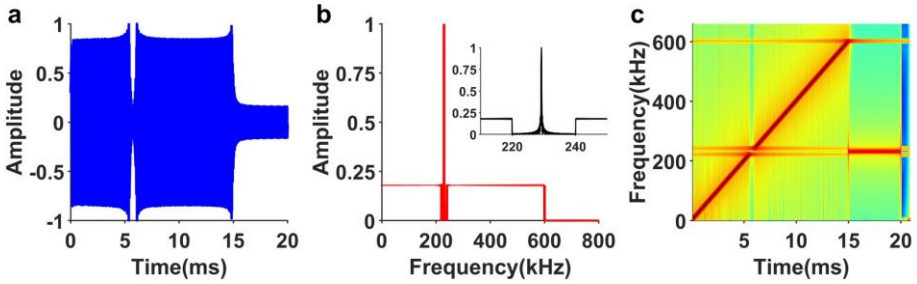

Figure 2. SWIFTSIN waveform with a notch from 220 kHz to 240 kHz and superposed a 229.2 kHz sinusoidal waveform. (a) Time domain waveform. (b) Magnitude spectrum. (c) Time-frequency spectrum.

RESULTS AND DISCUSSIONS

The SWIFT waveform isolation. When the isolation waveform is applied to the miniaturized ion trap mass spectrometer and the requirement for the isolation resolution is not high, the SWIFT waveform is usually the ideal choice. However, with the increasement of the isolation resolution, the SWIFT waveform will encounter some problems.

As illustrated in Figure 3, if we tried to isolate the isotope ion (labeled as A+1, at 358 m/z) of pioglitazone, the other isotope ions of it were labeled as A and A + 2, at 357 m/z and 359 m/z. The RF voltage at the full scan was 744 $V_{0\text{-}p}$ to 930 $V_{0\text{-}p}$, the frequency of the auxiliary AC was 200 kHz, and its amplitude was 0.5 $V_{0\text{-}p}$. Figure 3a plots the mass spectrum of 1 mg/L pioglitazone. For isolation process, the RF voltage was set to 828 $V_{0\text{-}p}$, the SWIFT waveform was set with a frequency band from 0 kHz to 600 kHz and, a notch from 198 kHz to 201 kHz, and the isolation duration was set to 21 ms.

To further improve the isolation resolution of the isotope ion A+1, two methods were tried. The first one was to narrow the notch band. For clearly illustrating the comparative results, we only reduced the notch band from one side, that is to say, the upper cut-off frequency of the notch band was adjusted from 201 kHz to 199.8 kHz and to 199.6 kHz respectively. Figure 3b plots the result of the target ion isolation after adjusting the notch frequency range. When the upper cut-off frequency was gradually reduced, the isotope ion A was gradually excited and the intensity decreased continuously. However, when the intensity of the isotope ion A remained about 3%, the intensity of the isotope ion A+1 lost 48%, which could be considered as the false excitation of the isotope ion A+1 caused by the notch band.

The second high-resolution isolation attempt was to increase the amplitude at the notch boundary. Again, only considering the excitation efficiency of the isotope A, we changed the amplitude at the upper cut-off frequency (201 kHz) to be 30 times and 35 times of the original. As can be seen from Figure 3c, with the increase of the amplitude of 201 kHz, the excitation efficiency of the isotope ion A was increasing. However, a similar situation also occurred, when the intensity of the isotope ion A remained at about 3%, the intensity of the A+1 isotope ion lost 33%. It could be suggested that the lack of the high-resolution isolation ability of the SWIFT waveform on a miniaturized mass spectrometer was mainly caused by the fact that the target ion can also absorb part of the energies in the notch band and get false excitation.

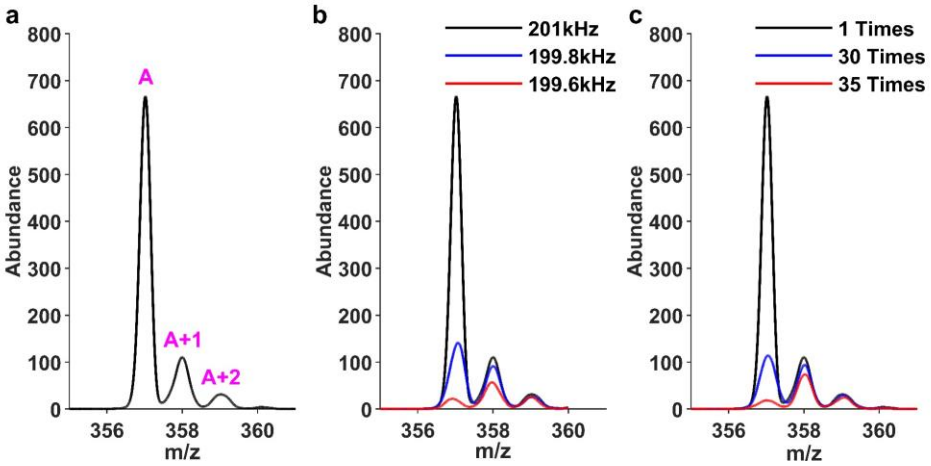

Figure 3. Isolation results using the SWIFT waveform, the sample is 1mg/L pioglitazone. (a) Isolation result using the SWIFT waveform with a notch band from 198 kHz to 201 kHz. (b) Isolation results using the SWIFT waveform after gradually narrowing the notch band. (c) Isolation results of the SWIFT waveform after changing the edge frequency amplitude of the notch frequency band.

Effective excitation frequency bandwidths. To verify the above conjecture, experiments were designed to explore the effective excitation frequency bandwidths of the ions with a specific mass-to-charge ratio, and the overlaps of the effective excitation frequency bandwidths of the adjacent ions. In particular, we applied a single sinusoidal waveform before scanning and the excitation efficiency can be defined as follows:

$$E\left(mz,\omega\right)=\frac{I_{full}\left(mz\right)-I_{\sin}\left(mz,\omega\right)}{I_{full}\left(mz\right)}\times 100\%, \tag{3}$$

where $I_{\sin}\left(mz,\omega\right)$ is the ion intensities with applying the sinusoidal excitation of frequency ω; $I_{full}\left(mz\right)$ is the full scanning ion intensities without the sinusoidal excitation; and $E\left(mz,\omega\right)$ represents the excitation efficiency, for a specific mass-to-charge ratio, it is a function of ω.

Similarly, taking 1 mg/L pioglitazone as the testing sample, when the frequency of the sinusoidal waveform changed from small to large, the isotope ions A + 2, A + 1, and A were excited orderly, as illustrated in Figure 4a (the duration of the sinusoidal waveform is 5 ms and the amplitude is 0.2 $V_{0\text{-}p}$). It can also be observed from Figure 4a that although the excitation efficiency almost reached 100% at the secular frequency of a specific ion, the adjacent frequency can also excite this ion effectively. Here, we define the effective excitation frequency bandwidth as the frequency region that the excitation efficiency is greater than or equal to 50% for a target ion.

By adjusting the duration and the amplitude of the sinusoidal waveform, the effective excitation frequency bandwidths also changed with these parameters. Figure 4b, 4c and 4d indicate the excitation efficiencies of the isotope ions A+2, A+1 and A at different frequencies when the excitation conditions were set to [2 ms, 0.5 $V_{0\text{-}p}$], [1 ms, 1 $V_{0\text{-}p}$] and [0.1 ms, 3 $V_{0\text{-}p}$] respectively. It can be observed from these results that the overlap of the effective excitation frequency bandwidths of the three isotope ions increased with the decreasing of the excitation duration and the increasing of the excitation amplitudes.

Figure 4e plots the frequency intervals from the point that isotope ion A+2 was first effectively excited to the point that A isotope ion was last effectively excited under different excitation conditions. It could be seen that with the increasing of the excitation amplitudes, the frequency intervals became larger. Figure 4f plots the overlap ratios of the effective excitation frequency bandwidths of the three isotope ions. We suggested that the increasing of the excitation amplitudes may bring an increasing in excitation energy, imply an increasing in

the effective excitation frequency bandwidths for each mass-to-charge ratio and cause the overlap of the effective excitation frequency bandwidths of the adjacent ions. An extreme case was that the effective excitation frequency bandwidths of the three ions all overlap. It was difficult to attempt to excite only the A isotope ion or the A + 1 isotope ion without affecting the adjacent ions, as shown in Figure 4d. To effectively excite the adjacent ions without reducing the intensity of the target ion, we should make the effective excitation frequency bandwidths of the adjacent ions overlap as little as possible. The parameters in Figure 4a set a footstone for such high-resolution excitation purpose. Using the frequency around 198 kHz, it was expected to realize the excitation of the isotope ion A+2 without affecting the isotope ion A+1. Similarly, using the frequency around 199.5 kHz, it was expected to realize the excitation of the isotope ion A without affecting the isotope ion A+1.

To further verify the above experimental results, we simulated the motion of ions with specific mass-to-charge ratio exciting by sinusoidal frequencies around its secular frequency. Figure S1a indicates that as the excitation frequency is close to the secular frequency, the amplitude of the ion motion increases, which can be used to confirm that part of the energies of the exciting frequency adjacent to secular frequency can also absorbed by the ions; this may cause by the intrinsic bandwidth of the exciting waveform. The closer to the secular frequency, the stronger the excitation ability. At the same time, it can explain the frequency bandwidth overlap phenomenon of adjacent ions being excited. Figure S1b shows that the larger the amplitude of the excitation waveform, the stronger the excitation capability. Figure S1c shows that the longer the duration of the excitation waveform, in a certain frequency range, the stronger the excitation capacity.

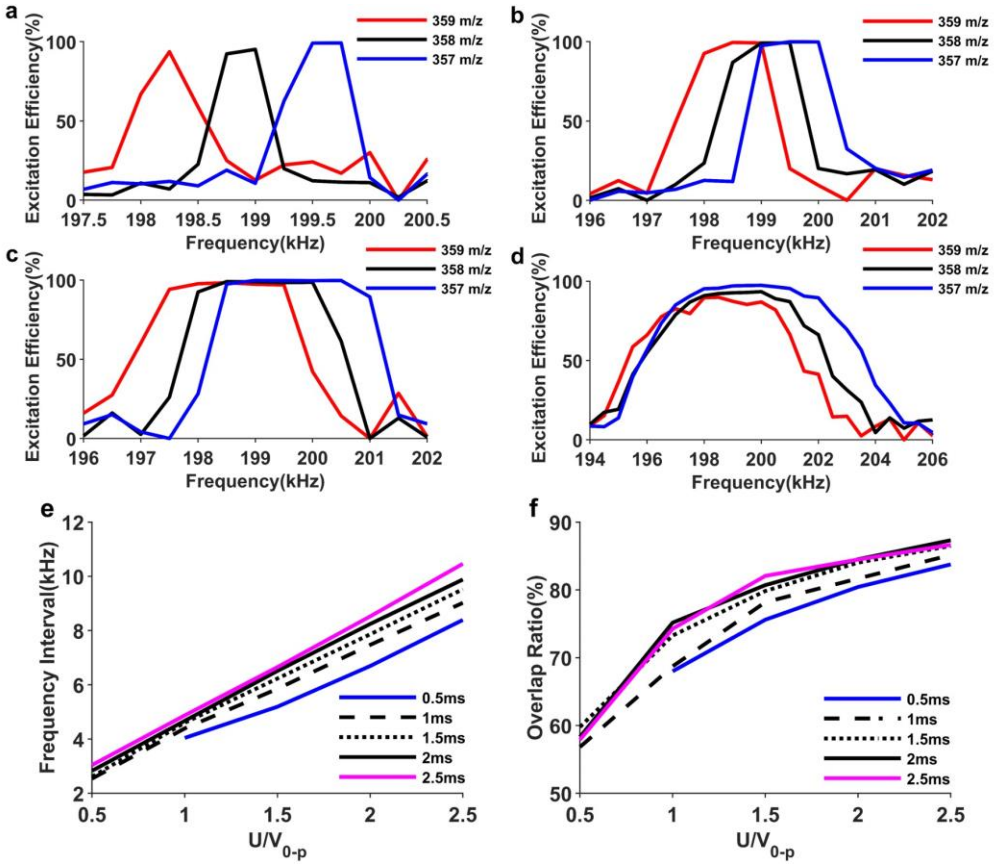

Figure 4. The excitation frequency bandwidths of the ions, the sample was 1mg/L pioglitazone. (a-d) The excitation efficiencies of the ions at different frequencies when the excitation conditions were 5 ms 0.2 $V_{0\text{-}p}$, 2 ms 0.5 $V_{0\text{-}p}$, 1 ms 1 $V_{0\text{-}p}$, 0.1 ms 3 $V_{0\text{-}p}$. (e) The frequency intervals from the A + 2 isotope ion were first effectively excited to the A isotope ion was last effectively excited under different excitation conditions. (f) The overlap ratios of the effective excitation frequency bandwidths of the ions with one mass-to-charge ratio (the average of three mass-to-charge ratio ions) under different excitation conditions.

The SWIFTSIN waveform isolation. Inspired by the above observations, the SWIFTSIN waveform was designed for the high-resolution isolation of the target ion. The sample was a mixture of promethazine hydrochloride (labeled as B at 317 m/z), rotonidine (labeled as C and at 356 m/z), rosiglitazone (labeled as D at 358 m/z) and repaglinide (labeled as E, at 453 m/z). All the samples were diluted in methanol to final concentrations of 1mg/L. The frequency of the auxiliary AC signal was 230 kHz, and the amplitude was 0.7 $V_{0\text{-}p}$. The full scan spectrum was shown in Figure 5a. It can be seen from the peaks of C and D that the spectral resolving power was poor without isolation. The SWIFT waveform with a notch from 227 kHz to 231 kHz and 2.5 $V_{0\text{-}p}$. was designed to roughly isolate rotonidine and rosiglitazone, and the resolution was significantly improved (inset of Figure. 5a). In addition to the isotope peak C and the isotope peak D, the isotope peaks of C + 1, D + 1 and D + 2 were also included.

High-resolution isolation means high-resolution excitation. Thus, in our experiments, we first kept the SWIFT parameters for coarse excitation as mentioned above, which the notch band of the waveform was designed as 227 kHz to 231 kHz, with an amplitude of 2.5 $V_{0\text{-}p}$ in the time domain; and then, the frequency of the superposed sinusoidal waveform was 229.2 kHz, and the amplitude was 0.27 $V_{0\text{-}p}$. The SWIFT waveform was compressed to the first 15 ms of the whole duration, and the sinusoidal waveform with a length of 5 ms was superposed on the latter half of the SWIFT waveform to achieve the purpose of coarse isolation to fine isolation. Figure 5b plots the isolation ability of the such SWIFTSIN waveform. It can be observed that the isotope ion C+1 was successfully excited, but the intensities of the adjacent ions were not affected. The inset of Figure 5b illustrates the isolation effect for a larger mass range, and it can be seen that ion B and E were effectively excited by the previous coarsely SWIFT waveform. It should be mentioned that, as shown in Figure 5b, the intensity of the isotope ion C+1 was not zero, but it retained a small part of the intensity. Even so, compared with the SWIFT waveform, which brought intensity loss up to 30% to the adjacent ions, the above excitation didn't affect the isotope ion C and D. Described by the previous mentioned overlap phenomenon of effective excitation frequency bandwidths, we suggested that the SWIFTSIN had obvious advantages.

Furthermore, figure 5c shows the ability to isolate the isotope ion D only using the SWIFTSIN waveform. For such purpose of unit mass isolation, the coarse notch of the SWIFT waveform was still designed to be 227 kHz to 231 kHz, but the difference was the superposition of four sinusoidal waveforms. The frequencies of the sinusoidal waveforms were 230 kHz, 229.2 kHz, 227.8 kHz, and 227.2 kHz, and the amplitudes were 0.23 $V_{0\text{-}p}$, 0.12 $V_{0\text{-}p}$, 0.12 $V_{0\text{-}p}$, and 0.23 $V_{0\text{-}p}$, respectively. They were used to excite isotope ions C, C + 1, D + 1, and D + 2. The red dashed line in Figure 5c shows that the isotope ion D is isolated without any loss of intensity. The above frequencies were the theoretical secular frequencies of the positive and negative two unit m/z adjacent to the isolation point, which were calculated from the quadrupole field model. This was just deducted from our hypothesis, that only frequency components near the isolation point will affect the isolation resolution finally. The excitation amplitudes were related to the injection volume, fine-tuned around 0.2 $V_{0\text{-}p}$ at small intervals and optimized in 0.01 $V_{0\text{-}p}$ steps. It can be argued that if the parameters of the quadrupole are defined, the related frequencies and amplitudes of our SINSWIFT waveform can also be easily fixed. It also can be considered to use a narrow SWIFT waveform for coarse isolation and superpose two sinusoidal waveforms (secular frequencies of one unit larger and one unit smaller of the isolation point), or to use a wider SWIFT waveform with more sinusoidal waveforms. However, the former setting may cause loss of target ions and the latter may cause leak of undesired adjacent ions. Thus, although we didn't optimize the configuration theoretically, the above parameters were optimal according to our current experiments.

We also applied collision-induced dissociation experiments to further prove that only the isotope ion D was isolated. The auxiliary AC signal for collision-induced dissociation was 50 kHz, and its amplitude was 0.15 $V_{0\text{-}p}$. The duration was 100 ms, and the RF voltage was 195 $V_{0\text{-}p}$ to 205 $V_{0\text{-}p}$. For comparison, the ions after only coarse isolation were fragmented. Figure 5d plots the MS/MS spectrum, where the isotope ion at m/z 135 corresponded to the fragment ion of rosiglitazone, and the isotope ions at m/z 165 and m/z 192 corresponded to the

fragment ions of rotundine.[39-42] In addition, the isotope ion at m/z 136 also appeared (blue line of the inset of Figure 5c), according to the fragmentation law, which can be considered that the ion was the fragmentation of the rosiglitazone isotope D+1. On the other hand, when the \isotope ion D obtained after fine isolation was fragmented, as indicated by the red dashed line of the inset of Figure 5c, the fragment peak was only retained at m/z 135 and other fragment peaks disappeared. It can be considered that the isolation of the isotope ion D was completed, and its intensity was not reduced.

Especially, it can be observed by comparing Figure 5d and Figure 5e that although the intensity of the isotope ion C+1 and the isotope ion D+1 may still be retained in a small part, this was not been reflected in the MS/MS spectrum.

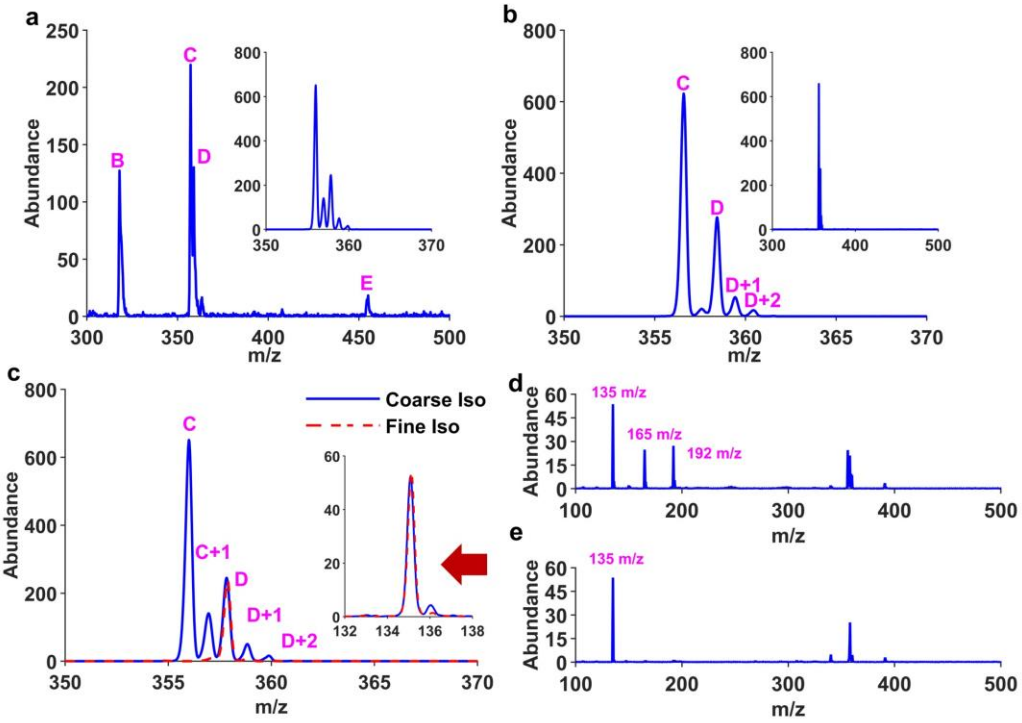

Figure 5. Isolation results using the SWIFTSIN waveform. The sample was a mixture of dioxypromazine hydrochloride, rotundine, rosiglitazone, and repaglinide, all samples were diluted in methanol to final concentrations of ~1mg/L. (a) Full scan spectrum. (b) Mass spectrum after the excitation of the isotope ions B, C+1, and E, the inset shows the spectrum of a larger mass range. (c) Mass spectrum after the isolation of the isotope ion D. (d) MS/MS spectrum after coarse isolation. (e) MS/MS spectrum after the isolation of the isotope ion D.

It is worth noting that when we designed the SWIFTSIN waveform, we used the most direct method to overlay a sinusoidal waveform onto the SWIFT waveform. The duration of the sinusoidal waveform was 5 ms. From the perspective of signal processing, the shorter the time is, the worse the resolution of the signal is. Therefore, the Gibbs effect could be observed in the notch of the amplitude spectrum of the SWIFTSIN waveform. However, when we used this direct superposition method to isolate the target ion, we did not find that the adjacent energy had any adverse effect on the target ion. Therefore, the isolation was completed by directly adding sinusoidal signals to the latter half of the isolated waveform.

Conclusion

In this paper, the efficiencies of ion excitation under different excitation conditions were explored, and the idea of effective excitation frequency bandwidths was proposed. With special attention to the overlap of effective excitation frequency bandwidths of the adjacent ions, the reason for the lack of the high-resolution ion isolation ability of the SWIFT waveform was analyzed. On this basis, a simple yet efficient isolation waveform, the SWIFTSIN operating in a coarse-to-fine manner, was proposed. Using this waveform, the unit mass isolation was realized on the miniaturized ion trap mass spectrometer without

reducing the intensity of the target ion. It can be expected to further achieve better isolation results under the condition of the higher performance of the instrument (such as allowing higher RF voltage). The high-resolution isolation can simplify MS/MS mass spectrum, help to improve the on-site detection efficiency of miniaturized mass spectrometry, and further help the researchers to understand the breaking pathway of compounds. This isolation technology is not only suitable for small-scale mass spectrometry, but also for any type of ion trap mass spectrometry. It puts forward a solution to improve the performance of mass spectrometers, especially the ion trap mass spectrometry whose physical structure has been determined.

Acknowledgement

This work was supported by National Natural Science Foundation of China (No. 22004079) and Shenzhen Natural Science Foundation (No. JCYJ20200109142824889)

References

1. Liu, H.; Yao, G. J.; Liu, X. K.; Liu, C.; Zhan, J.; Liu, D. H.; Wang, P.; Zhou, Z. Approach for Pesticide Residue Analysis for Metabolite Prothioconazole-desthio in Animal Origin Food. *J Agric Food Chem.* 2017, 65 (11), 2481-2487.
2. Khrushcheva, M. L.; Krivosheina, M. S.; Matveeva, M. D.; Zhilyaev, D. I.; Borisov, R. S. New Matrix Compounds for the Detection of Carboxyl-Containing Nonsteroidal Anti-Inflammatory Drugs by MALDI Mass Spectrometry. *Russ. J. Appl. Chem.* 2020, 93 (8), 1244-1253.
3. Scholl, P. F.; Gray, P. J.; Harp, B. P.; Delmonte, P. High resolution mass spectral data from the analysis of copper chlorophylls and copper chlorophyll degradation products in bright green table olives. *Data Brief.* 2020, 30, 105548.
4. Gonsalves, M. D.; Yevdokimov, A.; Brown-Nash, A.; Smith, J. L.; Oxley, J. C. Paper spray ionization-high-resolution mass spectrometry (PSI-HRMS) of peroxide explosives in biological matrices. *Anal Bioanal Chem*. 2021, 413 (11), 3069-3079.
5. Snyder, D. T.; Pulliam, C. J.; Ouyang, Z.; Cooks, R. G. Miniature and Fieldable Mass Spectrometers: Recent Advances. *Anal Chem.* 2016, 88 (1), 2-29.
6. Wang, X.; Zhou, X.; Ouyang, Z. Direct Analysis of Nonvolatile Chemical Compounds on Surfaces Using a Hand-Held Mass Spectrometer with Synchronized Discharge Ionization Function. *Anal Chem.* 2016, 88 (1), 826-831.
7. Li, G.; Li, D.; Cheng, Y.; Pei, X.; Zhang, H.; Wang, Y.; Sun, J.; Dong, M. Development of a low power miniature linear ion trap mass spectrometer with extended mass range. *Rev Sci Instrum*. 2017, 88 (12), 123108.
8. Pandey, S.; Hu, Y.; Bushman, L. R.; Castillo-Mancilla, J.; Anderson, P. L.; Cooks, R. G. Miniature mass spectrometer-based point-of-care assay for cabotegravir and rilpivirine in whole blood. *Anal Bioanal Chem*. 2022, 414 (11), 3387-3395.
9. Williams, J. D.; Cooks, R. G. Reduction of space-charging in the quadrupole ion trap by sequential injection and simultaneous storage of positively and negatively charged ions. *Rapid Commun. Mass Spectrom.* 1993, 7 (5), 380-382.
10. Tian, Y.; Higgs, J.; Li, A.; Barney, B.; Austin, D. E. How far can ion trap miniaturization go? Parameter scaling and space-charge limits for very small cylindrical ion traps. *J Mass Spectrom.* 2014, 49 (3), 233-240.
11. Jiang, T.; Xu, Q.; Zhang, H. J.; Li, D. Y.; Xu, W. Improving the Performances of a "Brick Mass Spectrometer" by Quadrupole Enhanced Dipolar Resonance Ejection from the Linear Ion Trap. *Anal. Chem.* 2018, 90 (19), 11671-11679.
12. Mielczarek, P.; Silberring, J.; Smoluch, M. Miniaturization in Mass Spectrometry. *Mass Spectrom Rev.* 2020, 39 (5-6), 453-470.
13. Acosta-Martin, A. E.; Coelho Graca, D.; Antinori, P.; Clerici, L.; Hartmer, R.; Meyer, M.; Hochstrasser, D.; Samii, K.; Lescuyer, P.; Scherl, A. Quantitative mass spectrometry analysis of intact hemoglobin A2 by precursor ion isolation and detection. *Anal Chem.* 2013, 85 (16), 7971-7975.
14. Xu, Z.; Jiang, T.; Xu, Q.; Zhai, Y.; Li, D.; Xu, W. Pseudo-Multiple Reaction Monitoring (Pseudo-MRM) Mode on the "Brick" Mass Spectrometer, Using the Grid-SWIFT Waveform. *Anal Chem.* 2019, 91 (21), 13838-13846.
15. Barr, J. M.; Van Stipdonk, M. J. Multi-stage tandem mass spectrometry of metal cationized leucine enkephalin and leucine enkephalin amide. *Rapid Commun Mass Spectrom.* 2002, 16 (6), 566-578.

16. Cousins, L. M.; Thomson, B. A. MS3 using the collision cell of a tandem mass spectrometer system. *Rapid Commun Mass Spectrom.* 2002, 16 (11), 1023-1034.
17. Tanaka, N.; Nagasaka, K.; Komatsu, Y. Selected Reaction Monitoring by Linear Ion-Trap Mass Spectrometry Can Effectively Be Applicable to Simultaneous Quantification of Multiple Peptides. *Biol. Pharm. Bull.* 2011, 34 (1), 135-141.
18. Schwartz, J. C.; Jaardine, I. High resolution parent-ion selection/isolation using a quadrupole ion-trap mass spectrometer. *Rapid Commun. Mass Spectrom.* 1992, 6 (4), 313-317.
19. Snyder, D. T.; Cooks, R. G. Ion isolation and multigenerational collision-induced dissociation using the inverse Mathieu q scan. *Rapid Commun. Mass Spectrom.* 2017, 31 (2), 200-206.
20. Wang, W.; Dong, M.; Song, C.; Cai, X.; Liu, Y.; Liu, Z.; Tian, S. Structural information of asphaltenes derived from petroleum vacuum residue and its hydrotreated product obtained by FT-ICR mass spectrometry with narrow ion isolation windows. *Fuel.* 2018, 227, 111-117.
21. Cataldi, T. R. I.; Lelario, F.; Orlando, D.; Bufo, S. A. Collision-Induced Dissociation of the A + 2 Isotope Ion Facilitates Glucosinolates Structure Elucidation by Electrospray Ionization-Tandem Mass Spectrometry with a Linear Quadrupole Ion Trap. *Anal. Chem.* 2010, 82 (13), 5686-5696.
22. Bianco, G.; Buchicchio, A.; Lelario, F.; Cataldi, T. R. Molecular formula analysis of fragment ions by isotope-selective collision-induced dissociation tandem mass spectrometry of pharmacologically active compounds. *J Mass Spectrom.* 2014, 49 (12), 1322-1329.
23. He, L.; Wu, J.-T.; Parus, S.; Lubman, D. M. Development of a capillary high-performance liquid chromatography tandem mass spectrometry system using SWIFT technology in an ion trap/reflectron time-of-flight mass spectrometer. *Rapid Commun. Mass Spectrom.* 1997, 11 (16), 1739-1748.
24. Murrell, J.; Konn, D. O.; Underwood, N. J.; Despeyroux, D. Studies into the selective accumulation of multiply charged protein ions in a quadrupole ion trap mass spectrometer. *Int. J. Mass Spectrom.* 2003, 227 (2), 223-234.
25. Ruddy, B. M.; Blakney, G. T.; Rodgers, R. P.; Hendrickson, C. L.; Marshall, A. G. Elemental composition validation from stored waveform inverse Fourier transform (SWIFT) isolation FT-ICR MS isotopic fine structure. *J Am Soc Mass Spectrom.* 2013, 24 (10), 1608-1611.
26. Ruddy, B. M. An investigation of deepwater horizon heavy end environmental transformation by high resolution detection and isolation Fourier transform ion cyclotron resonance mass spectrometry. Ph.D. Dissertation, University of Florida State, Gainesville, U.S., 2013.
27. Smith, D. F.; Blakney, G. T.; Beu, S. C.; Anderson, L. C.; Weisbrod, C. R.; Hendrickson, C. L. Ultrahigh Resolution Ion Isolation by Stored Waveform Inverse Fourier Transform 21 T Fourier Transform Ion Cyclotron Resonance Mass Spectrometry. *Anal Chem.* 2020, 92 (4), 3213-3219.
28. Kenny, D. V.; Callahan, P. J.; Gordon, S. M.; Stiller, S. W. Simultaneous isolation of two different m/z ions in an ion-trap mass spectrometer and their tandem mass spectra using filtered-noise fields. *Rapid Commun. Mass Spectrom.* 1993, 7 (12), 1086-1089.
29. Goeringer, D. E.; Asano, K. G.; McLuckey, S. A.; Hoekman, D.; Stiller, S. W. Filtered noise field signals for mass-selective accumulation of externally formed ions in a quadrupole ion trap. *Anal. Chem.* 1994, 66 (3), 313-318.
30. Hilger, R. T.; Santini, R. E.; Luongo, C. A.; Prentice, B. M.; McLuckey, S. A. A method for isolating ions in quadrupole ion traps using an excitation waveform generated by frequency modulation and mixing. *Int. J. Mass Spectrom.* 2015, 377, 329-337.
31. Sun, J.; Yan, H.; Li, D. A Method for Isolating Ions Using an Excitation Signal Generated by Superposing and Modulation Frequency. *2019 12th International Congress on Image and Signal Processing, BioMedical Engineering and Informatics (CISP-BMEI)*. 2019, pp 1-5.
32. Guan, S. H. General phase modulation method for stored waveform inverse Fourier transform excitation for Fourier transform ion cyclotron resonance mass spectrometry. *J. Chem. Phys.* 1989, 91 (2), 775-777.
33. Guan, S. Optimal phase modulation in stored waveform inverse Fourier transform excitation for Fourier transform mass spectrometry. II. Magnitude spectrum smoothing. *J. Chem. Phys.* 1990, 93 (12), 8442-8445.
34. Guan, S. H.; Marshall, A. G. Stored waveform inverse Fourier transform (SWIFT) ion excitation in trapped-ion mass spectometry: Theory and applications. *Int. J. Mass Spectrom.* 1996, 157, 5-37. 35. Soni, M. H.; Cooks, R. G. Selective injection and isolation of ions in quadrupole ion-trap mass-spectrometry using notched wave-forms created using the inverse fourier-transform. *Anal. Chem.* 1994, 66 (15), 2488-2496.

36. Doroshenko, V. M.; Cotter, R. J. Advanced stored waveform inverse Fourier transform technique for a matrix-assisted laser desorption/ionization quadrupole ion trap mass spectrometer. *Rapid Commun. Mass Spectrom.* 1996, 10 (1), 65-73.
37. Zhang, X. H.; Huo, X. M.; Tang, F.; Zha, Z. Y.; Yang, F. B.; Ni, Y. F.; Wang, Y. J.; Zhou, M. F.; Wang, X. H. Characterisation and optimisation of ion discrimination in a mini ion funnel for a miniature mass spectrometer. *Anal. Methods.* 2019, 11 (19), 2551-2558.
38. Huo, X.; Zhu, X.; Tang, F.; Zhang, J.; Zhang, X.; Yu, Q.; Wang, X. Discontinuous Subatmospheric Pressure Interface Reduces the Gas Flow Effects on Miniature CAPI Mass Spectrometer. *Anal. Chem.* 2020, 92 (5), 3707-3715.
39. Chou, C. C.; Lee, M. R.; Cheng, F. C.; Yang, D. Y. Solid-phase extraction coupled with liquid chromatography-tandem mass spectrometry for determination of trace rosiglitazone in urine. *Journal of Chromatography A.* 2005, 1097 (1-2), 74-83.
40. Zhuang, X.; Lin, Q.; Li, C.; Deng, J.; Li, H. In vitro comparison of rotundine metabolism in liver microsomes of human,dog and rat. *Chin. Pharmacol. Bull.*. 2009, 25 (9), 1147-1152.
41. Yu, F. F.; Lv, H. N.; Dong, W. J.; Ye, J.; Hao, H. Z.; Ma, S. G.; Yu, S. S.; Liu, Y. L. Development and validation of a liquid chromatography-tandem mass spectroscopy method for simultaneous determination of (+)-(13aS)-deoxytylophorinine and its pharmacologically active 3-O-desmethyl metabolite in rat plasma. *J. Pharm. Biomed. Anal.* 2015, 107, 223-228.
42. Rashid, J.; Ahsan, F. A highly sensitive LC-MS/MS method for concurrent determination of sildenafil and rosiglitazone in rat plasma. *J. Pharm. Biomed. Anal.* 2016, 129, 21-27.